

LA-UR-21-26105

Accepted Manuscript

Asynchronous Truncated Multigrid-Reduction-in-Time

Hahne, Jens

Southworth, Benjamin Scott

Friedhoff, Stephanie

Provided by the author(s) and the Los Alamos National Laboratory (2024-09-16).

To be published in: SIAM Journal on Scientific Computing

DOI to publisher's version: 10.1137/21M1433149

Permalink to record:

<https://permalink.lanl.gov/object/view?what=info:lanl-repo/lareport/LA-UR-21-26105>



Los Alamos National Laboratory, an affirmative action/equal opportunity employer, is operated by Triad National Security, LLC for the National Nuclear Security Administration of U.S. Department of Energy under contract 89233218CNA000001. By approving this article, the publisher recognizes that the U.S. Government retains nonexclusive, royalty-free license to publish or reproduce the published form of this contribution, or to allow others to do so, for U.S. Government purposes. Los Alamos National Laboratory requests that the publisher identify this article as work performed under the auspices of the U.S. Department of Energy. Los Alamos National Laboratory strongly supports academic freedom and a researcher's right to publish; as an institution, however, the Laboratory does not endorse the viewpoint of a publication or guarantee its technical correctness.

ASYNCHRONOUS TRUNCATED MULTIGRID-REDUCTION-IN-TIME (AT-MGRIT)*

JENS HAHNE[†], BEN S. SOUTHWORTH [‡], AND STEPHANIE FRIEDHOFF [†]

Abstract. In this paper, we present the new “asynchronous truncated multigrid-reduction-in-time” (AT-MGRIT) algorithm for introducing time parallelism to the solution of discretized time-dependent problems. The new algorithm is based on the multigrid-reduction-in-time (MGRIT) approach, which, in certain settings, is equivalent to another common multilevel parallel-in-time method, Parareal. In contrast to Parareal and MGRIT that both consider a global temporal grid over the entire time interval on the coarsest level, the AT-MGRIT algorithm uses truncated local time grids on the coarsest level, each grid covering certain temporal subintervals. These local grids can be solved completely in an independent way from each other, which reduces the sequential part of the algorithm and, thus, increases parallelism in the method. Here, we study the effect of using truncated local coarse grids on the convergence of the algorithm, both theoretically and numerically, and show, using challenging nonlinear problems, that the new algorithm consistently outperforms classical Parareal/MGRIT in terms of time to solution.

16 **Key words.** Parallel-in-time integration, Parareal, MGRIT, truncated coarsest grids

17 AMS subject classifications. 65F10, 65M22, 65M55

18 **1. Introduction.** Time-dependent problems are classically solved by a time-
 19 stepping procedure that propagates the solution stepwise forward in time. The method
 20 is optimal, i. e., of order $\mathcal{O}(N_t)$ for N_t time steps. However, this method quickly be-
 21 comes a parallel bottleneck when using modern computer architectures, which have
 22 an increasing number of processors, yet stagnating processor clock speed. Due to
 23 the sequential nature of classical time stepping, parallelization is limited to the spa-
 24 tial domain, and, as the number of processors grows, spatial parallelization becomes
 25 exhausted even if more resources are available. Parallel-in-time methods use these
 26 resources of modern computer architectures to compute multiple time steps simulta-
 27 neously, enabling spatial *and* temporal parallelization.

The development of the first parallel-in-time method goes back over 50 years [30], and an overview of the field can be found in [13]. Two of the best known methods are the Parareal method [24] and the multigrid-reduction-in-time (MGRIT) algorithm [11], both of which are based on multigrid reduction principles [33] applied in the time dimension. Parareal can be interpreted as a two-level multigrid method, and MGRIT generalizes the approach to a multilevel setting. The ideas of both methods are similar, and both methods are equivalent in certain settings. On the “fine” level(s), time integration is simultaneously (i.e., in parallel) applied to non-overlapping temporal subdomains, and on the coarsest level, the entire time interval is solved with sequential time stepping. The choice of the number of levels and the choice of the coarsest grid is both critical and challenging. The typical choice of the coarse grid in the two-level setting is based on the number of processes, choosing as many points on the coarse grid as there are processes available [24]. With this strategy, the fine level can be perfectly parallelized, but for a large number of processes, the

*Submitted to the editors DATE.

Funding: This work is supported by the BMBF (project PASIROM; grant 05M18PXB). BSS was supported as a Nicholas C. Metropolis Fellow under the Laboratory Directed Research and Development program of Los Alamos National Laboratory.

[†]Department of Mathematics, Bergische Universität Wuppertal, Germany (jens.hahne@math.uni-wuppertal.de, friedhoff@math.uni-wuppertal.de).

[‡]Theoretical Division, Los Alamos National Laboratory, USA (southworth@lanl.gov).

42 serial work on the coarsest level dominates the runtime.

43 Strategies to reduce the runtime of two-level schemes include variants of the
 44 Parareal algorithm, such as asynchronous Parareal [39, 26], a modified version en-
 45 hanced by the asynchronous iterative scheme [6], or an adaptive Parareal algorithm,
 46 which increases the accuracy of the fine solver over the Parareal iterations. Using
 47 more than two grid levels can significantly reduce the serial work by using a coarsest
 48 grid with only a few time points, but the resulting very large time steps can be very
 49 expensive, if not infeasible, to compute for some applications [4] and/or may affect
 50 the convergence of the algorithm [8].

51 MGRIT and Parareal are primarily effective on parabolic-type problems [31, 37],
 52 which have a naturally dissipative behavior over long time intervals. Here, we make
 53 the observation that, due to the dissipative behavior inherent to these problems, the
 54 coarsest grid probably does *not* need to represent the full time domain. Indeed, the
 55 solution at time $t = 0$ will often have a negligible effect on the solution at much later
 56 times. Thus, in many cases we believe that computing a global coarse grid introduces
 57 an unnecessary sequential computational effort to an otherwise parallel algorithm.

58 In this paper, we introduce a new way to define the coarsest level in Parareal and
 59 MGRIT, emphasizing reducing the serial work while avoiding large time steps. Instead
 60 of solving the entire time interval serially on the coarsest grid, we define multiple
 61 *independent local* coarse grids each consisting of k coarse-grid time points that can be
 62 propagated independently and simultaneously. This idea was originally motivated by
 63 similar processor-local multigrid hierarchies used in geometric and algebraic multigrid
 64 for elliptic problems [2, 27, 28]. Such an approach offers both improved parallelism
 65 and reduced computational cost compared with a global coarse-grid solve, while still
 66 providing sufficient coarse-level information to each processor for rapid convergence
 67 of the global problem. Due to the asynchronous nature of computing the truncated
 68 coarsest grids, we refer to the new algorithm as “asynchronous truncated MGRIT”
 69 (AT-MGRIT).

70 Section 2 introduces the algorithm in a two-level and multilevel context, providing
 71 an FAS interpretation of the multilevel variant in Algorithm 2.2. In Section 3, we an-
 72 alyze the new algorithm theoretically, derive two-level error propagators, and present
 73 two-level convergence bounds in Subsection 3.2. We then describe various properties
 74 of the algorithm in Section 4, including describing the implementation with associ-
 75 ated communication scheme in Subsection 4.1 and performing a parameter study for
 76 a model problem in Subsection 4.3. Finally, we apply the new algorithm to two chal-
 77 lenging nonlinear problems, a chemical reaction in Subsection 5.1 and the simulation
 78 of a realistic model of an electrical machine in Subsection 5.2. AT-MGRIT consis-
 79 tently offers a 5–30% reduction in wallclock time compared with traditional MGRIT
 80 and Parareal, and we expect the speedup to be greater if the algorithms were applied
 81 on GPUs.

82 **2. An overlapping and asynchronous coarse grid.** Consider an initial value
 83 problem of the form

$$84 \quad (2.1) \quad \mathbf{u}'(t) = \mathbf{f}(t, \mathbf{u}(t)), \quad \mathbf{u}(t_0) = \mathbf{g}_0, \quad t \in (t_0, t_f].$$

85 We discretize (2.1) on a uniformly-spaced temporal grid $t_i = i\Delta t$, $i = 0, 1, \dots, N_t$,
 86 with constant step size $\Delta t = (t_f - t_0)/N_t$, and let $\mathbf{u}_i \approx \mathbf{u}(t_i)$ for $i = 0, \dots, N_t$
 87 with $\mathbf{u}_0 = \mathbf{u}(0)$. A general form of a single step time integration method for the
 88 time-discrete initial value problem is

$$89 \quad (2.2) \quad \mathbf{u}_i = \Phi_i(\mathbf{u}_{i-1}) + \mathbf{g}_i, \quad i = 1, 2, \dots, N_t,$$

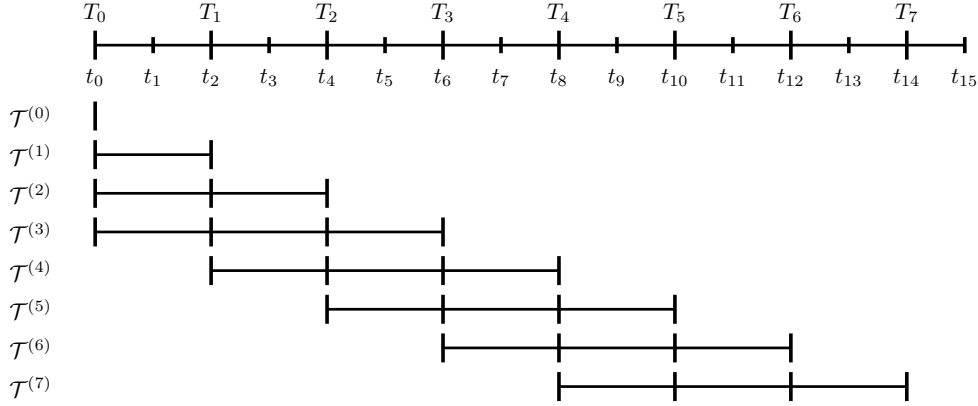


Fig. 1: Two-level temporal grid-hierarchy example for the AT-MGRIT algorithm with $N_t = 15$, $m = 2$ and $k = 4$. The C -points (long markers) define the global coarse grid. For each point $p = 0, \dots, 7$ on the global coarse grid, a local coarse grid $\mathcal{T}^{(p)}$ is created.

90 where Φ_i is a one-step time integrator, propagating a solution \mathbf{u}_{i-1} from a time point
 91 t_{i-1} to time point t_i , and \mathbf{g}_i contains forcing terms. Equation (2.2) can be written as
 92 a semi-linear matrix equation

$$93 \quad A(\mathbf{u}) \equiv \begin{bmatrix} I & & & & \\ -\Phi_1(\cdot) & I & & & \\ \ddots & \ddots & \ddots & & \\ & & & -\Phi_{N_t}(\cdot) & I \end{bmatrix} \begin{bmatrix} \mathbf{u}_0 \\ \mathbf{u}_1 \\ \vdots \\ \mathbf{u}_{N_t} \end{bmatrix} = \begin{bmatrix} \mathbf{g}_0 \\ \mathbf{g}_1 \\ \vdots \\ \mathbf{g}_{N_t} \end{bmatrix} \equiv \mathbf{g},$$

94 where $\Phi_i(\cdot)$ indicates that Φ_i is nonlinearly evaluated at the corresponding (block)
 95 vector entry. This system can be solved by a (linear) sequential block forward solve.

96 In contrast, the iterative AT-MGRIT algorithm solves the problem by updating
 97 multiple time points simultaneously. In the following, we first introduce the idea of
 98 the algorithm in Subsection 2.1 for the two-level case and explain how the algorithm
 99 works. We then discuss how the two-level method can be extended to a multilevel
 100 setting.

101 **2.1. Two-level AT-MGRIT algorithm.** For a given time grid $t_i = i\Delta t, i = 0, 1, \dots, N_t$, and a given coarsening factor $m > 1$, we define a splitting of all time-points
 102 into F - and C -points, such that every m -th point is a C -point (note, non-uniform
 103 coarsening is also possible; uniform coarsening is used here to simplify presentation).
 104 This defines a global coarse grid of C -points $T_i = i\Delta T, i = 0, 1, \dots, N_T$, with time step
 105 $\Delta T = m\Delta t$; all other non- C -points are F -points. Based on this global coarse grid,
 106 we define $N_T + 1$ overlapping *local* coarse grids. Given local grid size k , the p th local
 107 coarse grid, $\mathcal{T}^{(p)}$ for $p = 0, \dots, N_T$, is given by

$$109 \quad \mathcal{T}^{(p)} = \{i\Delta T : i \in [\max(0, p - k + 1), p]\},$$

110 with time step size $\Delta T = m\Delta t$, as depicted in Figure 1.

111 The two-level AT-MGRIT algorithm uses this time-grid hierarchy to solve time-
 112 dependent problems of the form (2.2) and is based on the following procedure: Given

114 an initial solution \mathbf{u} and the right-hand side \mathbf{g} , the first step of the algorithm applies a
 115 block relaxation, the so-called F -relaxation, to the fine space-time system of equations
 116 $A\mathbf{u} = \mathbf{g}$. The F -relaxation propagates the solution from a C -point to all following
 117 F -points preceding the next C -point (analogously to standard MGRIT/Parareal [11]).
 118 The relaxation of each interval of F -points can be executed in parallel and consists
 119 of $m - 1$ sequential applications of the time integrator. In the next step, the global
 120 residual vector \mathbf{r} is computed and restricted by injection ($R_I^{(p)}$) to all local coarse grids.
 121 For each local coarse grid, the coarse system $A_c^{(p)} \mathbf{u}_c^{(p)} = \mathbf{r}_c^{(p)}$ is solved, which consists
 122 of $k - 1$ sequential applications of the coarse time integrator. Since the coarse-grid
 123 problems are independent of each other, they can be solved simultaneously. Then,
 124 the global solution vector is corrected using “selective ideal” interpolation, $P_S^{(p)}$. The
 125 selective ideal interpolation is the transpose of an injection followed by an F -relaxation
 126 starting from exactly one point in time. More precisely, the approximation of the
 127 solution at the last time point of each local coarse grid is interpolated to the fine grid
 128 and then, an F -relaxation is performed using these interpolated points. The steps are
 129 applied iteratively until a desired quality of the solution is achieved. The two-level
 130 AT-MGRIT algorithm is summarized in [Algorithm 2.1](#).

Algorithm 2.1 AT-MGRIT ($A, \mathbf{u}, \mathbf{g}$)

```

1: repeat
2:   Apply  $F$ -relaxation to  $A\mathbf{u} = \mathbf{g}$ 
3:   Compute residual  $\mathbf{r} = \mathbf{g} - A\mathbf{u}$ 
4:   For  $p = 0$  to  $N_T$ :
5:     Restrict residual,  $\mathbf{r}_c^{(p)} = R_I^{(p)}\mathbf{r}$ 
6:     Solve local system  $A_c^{(p)} \mathbf{u}_c^{(p)} = \mathbf{r}_c^{(p)}$ 
7:     Correct using  $\mathbf{u} = \mathbf{u} + P_S^{(p)} \mathbf{u}_c^{(p)}$ 
8: until stopping criterion is reached
  
```

131 We follow the typical MGRIT notation here and therefore specify the F -relaxation
 132 in line 2. From the second iteration on, this F -relaxation can be skipped, since the up-
 133 dates are already performed as part of the selective ideal interpolation of the previous
 134 iteration. Note, that the AT-MGRIT algorithm solves for the exact solution in N_T
 135 iterations if $k > 1$. Furthermore, the algorithm is equivalent to the Parareal method if
 136 $k = N_T + 1$, i. e., if all local coarse grids contain all C -points before in time. All com-
 137 ponents of the AT-MGRIT algorithm are highly parallel. The only communication
 138 needed is for the residual computation and the distribution of the residual (performed
 139 by the matrix-vector product $\mathbf{r}_c^{(p)} = R_I^{(p)}\mathbf{r}$ in [Algorithm 2.1](#)). Moreover, the coarse-
 140 level solve is communication-free (except for any communication that arises in spatial
 141 parallelism). This is particularly relevant for emerging heterogeneous computing ar-
 142 chitectures, where communication to and from GPU nodes can be quite expensive,
 143 and high efficiency is obtained with a low communication to computation ratio. For
 144 the coarse time integrator Φ_{i_c} , here we choose a re-discretization of the problem with
 145 step size ΔT , but other choices such as coarsening in space [34, 25, 20] or order of
 146 discretization [29, 12] can also be used.

147 **2.2. Multilevel FAS AT-MGRIT algorithm.** The two-level AT-MGRIT al-
 148 gorithm can easily be extended to the multilevel setting and the full approximation
 149 storage (FAS) framework [5] can be used to solve both linear and nonlinear problems.
 150 Analogously to MGRIT, a multilevel hierarchy of temporal grids is constructed recur-

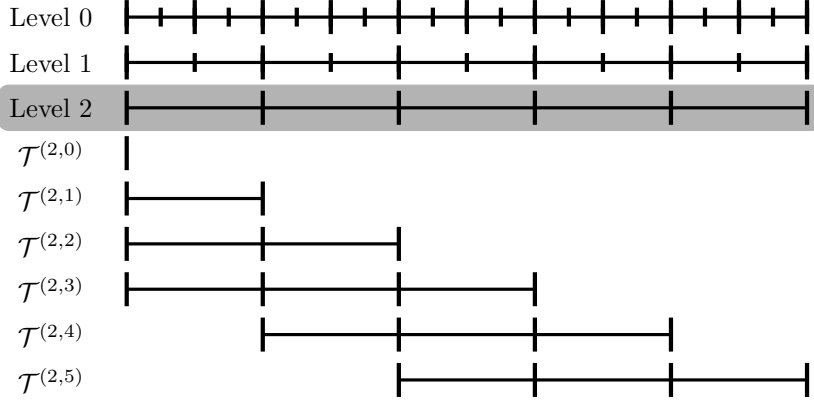


Fig. 2: Example of a three-level time grid hierarchy for the AT-MGRIT algorithm for a fine grid with 21 time points, $m = 2$ and $k = 4$. At the coarsest level, a local coarse grid is generated for each C -point of the global coarse grid (gray box). These local grids ($\mathcal{T}^{(2,p)}$, $p = 0, \dots, 5$) replace the global coarse grid used in the classical MGRIT algorithm.

151 sively using a uniform or non-uniform coarsening strategy. AT-MGRIT uses the same
 152 levels, coarsening, relaxation, and transfer operators as MGRIT on all finer levels
 153 in the hierarchy, but the coarsest MGRIT grid is replaced by local grids. Figure 2
 154 shows an example grid hierarchy for three-level AT-MGRIT with $N_t = 20$, $m = 2$,
 155 and $k = 4$. While MGRIT utilizes the global coarse grid on level 2, AT-MGRIT uses
 156 local grids $\mathcal{T}^{(2,p)}$, $p = 0, \dots, 5$.

157 In the following, we assume that all problem-dependent forcing terms are in-
 158 cluded in the time integrator. Then, the multilevel FAS AT-MGRIT V -cycle algo-
 159 rithm is given in Algorithm 2.2, where $N_t^{(\ell)}$ denotes the number of time points, and
 160 $\mathcal{A}^{(\ell)}\mathbf{u}^{(\ell)} = \mathbf{g}^{(\ell)}$ and $\mathcal{A}^{(\ell,p)}\mathbf{u}^{(\ell,p)} = \mathbf{g}^{(\ell,p)}$ specifies the space-time system of equations
 161 on levels $\ell = 0, 1, \dots, L - 1$ and on the local coarse grids $p = 0, 1, \dots, N_t^{(\ell)}$, respec-
 162 tively. On all except for the coarsest level, we use restriction by injection ($R_I^{(\ell)}$),
 163 “ideal” interpolation ($P^{(\ell)}$), and $F(CF)^\nu$ -relaxation. For more details on MGRIT
 164 (and thus AT-MGRIT on finer levels), see [11]. At the coarsest level, restriction and
 165 interpolation to and from the local coarse grids is done by injection, denoted by $R_I^{(\ell,p)}$
 166 and $P_I^{(\ell,p)}$, respectively. Note that at the coarsest level, the residual is first trans-
 167 ferred to the global coarse grid and then to the local coarse grids, allowing for a nicer
 168 notation of the algorithm. AT-MGRIT can also be used with other common MGRIT
 169 cycle types, such as F -cycles [38] or nested iterations [23, 22]. While F -cycles visit
 170 the coarsest level several times per iteration, nested iterations compute an improved
 171 initial guess by starting on the coarsest level and interpolating the solution to the
 172 finer levels, applying one V -cycle per level. For all cycle types, the standard MGRIT
 173 coarsest level can be replaced by local coarse grids. Analogous to the two-level setting,
 174 AT-MGRIT is equivalent to MGRIT if $k = N_t^{(L-1)} + 1$.

176 **3. Theory.** This section develops convergence theory for AT-MGRIT in the lin-
 177 ear two-level setting. The analysis is built on two-level MGRIT/Parareal theory devel-
 178 oped in [9, 36], and gives insight on the effects of truncating the coarse-grid time grid.

Algorithm 2.2 AT-MGRIT FAS(ℓ)

```

1: repeat
2:   if  $\ell$  is the coarsest level:
3:     For  $p = 0$  to  $N_t^{(\ell)}$ :
4:       Restrict to local grids
5:        $\mathbf{v}^{(\ell,p)} = R_I^{(\ell,p)}(\mathbf{v}^{(\ell)})$ 
6:        $\mathbf{g}^{(\ell,p)} = R_I^{(\ell,p)}(\mathbf{g}^{(\ell)})$ 
7:       Solve local problem  $\mathcal{A}^{(\ell,p)}(\mathbf{u}^{(\ell,p)}) = \mathcal{A}^{(\ell,p)}(\mathbf{v}^{(\ell,p)}) + \mathbf{g}^{(\ell,p)}$ 
8:       Update  $\mathbf{u}^{(\ell)} = P_I^{(\ell,p)} \mathbf{u}^{(\ell,p)}$ 
9:     else
10:      Apply  $F$ -relaxation to  $\mathcal{A}^{(\ell)}(\mathbf{u}^{(\ell)}) = \mathbf{g}^{(\ell)}$ 
11:      For 0 to  $\nu$ :
12:        Apply  $CF$ -relaxation to  $\mathcal{A}^{(\ell)}(\mathbf{u}^{(\ell)}) = \mathbf{g}^{(\ell)}$ 
13:      Inject the approximation and its residual to the coarse grid
14:       $\mathbf{u}^{(l+1)} = R_I^{(\ell)}(\mathbf{u}^{(\ell)})$ 
15:       $\mathbf{v}^{(l+1)} = \mathbf{u}^{(l+1)}$ 
16:       $\mathbf{g}^{(l+1)} = R_I^{(\ell)}(\mathbf{g}^{(\ell)} - \mathcal{A}^{(\ell)} \mathbf{u}^{(\ell)})$ 
17:      Solve on next level: AT-MGRIT ( $\ell + 1$ )
18:      Compute the error approximation:  $\mathbf{e} = \mathbf{u}^{(\ell+1)} - \mathbf{v}^{(\ell+1)}$ 
19:      Correct using ideal interpolation:  $\mathbf{u}^{(\ell)} = \mathbf{u}^{(\ell)} + P^{(\ell)}(\mathbf{e})$ 
20: until stopping criterion is reached

```

179 We begin by introducing the error-propagation operator in the case of exact solves
 180 on a truncated coarse grid (Subsection 3.1.1) and inexact coarse-grid solves (Sub-
 181 section 3.1.2). Formal two-level convergence bounds are provided in Subsection 3.2.
 182 Because we are in the two-level setting, we drop ℓ superscripts from Subsection 2.2.

183 **3.1. Error propagation.** Following from [11], the two-level error propagation
 184 operator for linear AT-MGRIT with an exact coarse-grid solve is given by:

185 (3.1)
$$\mathcal{E} := \left(I - \sum_{p=0}^{N_T} P_S^{(p)} (A_c^{(p)})^{-1} R_I^{(p)} A \right) P R_I,$$

 186

187 where $A_c^{(p)}$ represents the local coarse grid systems, $R_I^{(p)}$ is the restriction operator to
 188 the local coarse grids, and $P_S^{(p)}$ defines the interpolation from the local coarse grids
 189 that updates the fine grid using *selective ideal interpolation*, i. e., for one specific C -
 190 point, this C -point and the following interval of F -points are updated. We see that
 191 (3.1) is analogous to that derived in [11, Eq. 2.12], but here we must sum over C -
 192 points, as each C -point is updated by a unique local coarse-grid. The operators P
 193 and R_I , corresponding to ideal interpolation and restriction by injection, respectively,
 194 are given by

$$\begin{aligned}
195 \quad P &:= I \otimes \begin{bmatrix} I \\ \Phi \\ \vdots \\ \Phi^{m-1} \end{bmatrix}^m, \\
R_I &:= \begin{bmatrix} I & & & \\ \mathbf{0} & \cdots & \mathbf{0} & I \\ & \ddots & & \\ & & \mathbf{0} & \cdots & \mathbf{0} & I \end{bmatrix}_{N_T}, \\
P_S^{(p)} &:= \begin{bmatrix} I \\ \Phi \\ \vdots \\ \Phi^{m-1} \end{bmatrix}_{\min(p, k-1)}^m.
\end{aligned}$$

196 Note, that the operator PR_I is equivalent to error propagation for F -relaxation [11].
197 Recall that the fine-grid operator has block dimension $(N_t + 1) \times (N_t + 1)$, with each
198 block being a square operator the size of Φ . Letting $N_t = mN_T$ for coarse-grid points
199 $0, \dots, N_T$, the fine-grid size can be written as $(mN_T + 1) \times (mN_T + 1)$, which we will
200 use to express error propagation largely in terms of $m \times m$ coarse blocks. Each of
201 these blocks represents a block of one C -point and $m - 1$ following F -points. At the
202 end, there is a single block containing only one C -point. Note that the structure
203 for this block is always a submatrix of the $m \times m$ blocks, containing only the part
204 corresponding to the C -point.

205 **3.1.1. Exact local coarse grid solve.** First, we consider the effect of the local
206 coarse grids using exact solves on the coarse time steps. For this purpose, we define
207 the local coarse-grid problem as

$$208 \quad A_c^{(p)} := R_I^{(p)} AP^{(p)},$$

210 where $P^{(p)}$ and $R_I^{(p)}$ define the transfer between the fine grid and the local coarse
211 grids and are submatrices of P and R_I . For $P^{(p)}$, only columns of P associated to
212 points lying on this local coarse grid are considered. Equivalently, only the associated
213 rows are considered for the restriction. Then, the coarse-grid problems are given by

$$214 \quad R_I^{(p)} AP^{(p)} = \begin{bmatrix} I & & & \\ -\Phi^m & I & & \\ & -\Phi^m & I & \\ & & \ddots & \ddots \\ & & & -\Phi^m & I \end{bmatrix}_{\min(p+1, k)}.$$

215 Here, it is important to note that all local coarse-grid systems $R_I^{(p)} AP^{(p)}$ have the
216 same structure, but consider different time intervals. In fact, the exact local coarse-
217 grid systems are principal submatrices of the Schur complement corresponding to a
218 standard Parareal/MGRIT coarse-grid with exact solves [11].

219 We can now examine the error-propagator \mathcal{E}_e using exact solves on the local coarse
220 grids. We refer to [Appendix A](#) for detailed algebraic derivations. In forming \mathcal{E}_e by
221 summing over $p = 1, \dots, N_T$, we obtain a block lower triangular matrix, whereby each

222 p updates m rows of \mathcal{E} , and the error-propagator using ideal local coarse grids can be
 223 written in block form as

(3.2)

$$224 \quad \mathcal{E}_e = \begin{bmatrix} \mathbf{0} & \cdots & \mathbf{0} \\ \vdots & \cdots & \vdots \\ \mathbf{0} & \cdots & \mathbf{0} \\ \mathcal{G} & \mathbf{0} & \cdots & \mathbf{0} \\ \mathbf{0} & \ddots & \ddots & \vdots \\ \mathbf{0} & \mathbf{0} & \mathcal{G} & \mathbf{0} & \cdots & \mathbf{0} \\ \mathbf{0} & \mathbf{0} & \mathbf{0} & \bar{\mathcal{G}} & \mathbf{0} & \cdots & \mathbf{0} \end{bmatrix}_1 \quad \mathcal{G} = \begin{bmatrix} \Phi^{km} & \mathbf{0} & \cdots & \mathbf{0} \\ \Phi^{km+1} & \mathbf{0} & \cdots & \mathbf{0} \\ \vdots & \vdots & \vdots & \vdots \\ \Phi^{km+m-1} & \mathbf{0} & \cdots & \mathbf{0} \end{bmatrix}_m, \quad \bar{\mathcal{G}} = \left[\Phi^{km} \mathbf{0} \cdots \mathbf{0} \right]_1,$$

225 where $\bar{\mathcal{G}}$ is identical to the first row of \mathcal{G} and represents the additional block con-
 226 sisting of one C -point. Note that the error propagator \mathcal{E}_e is nonzero, so unlike
 227 Parareal/two-level MGRIT, AT-MGRIT using exact local coarse-grid inverses is not
 228 a direct method. For all $p > k$, we have some error perturbation that results from
 229 truncating the exact (Schur-complement) coarse grid.

230 **3.1.2. Approximate local coarse grid solve.** As typical for multigrid reduc-
 231 tion techniques, we do not invert $R_I^{(p)} AP^{(p)}$ exactly, but approximate $R_I^{(p)} AP^{(p)} \approx$
 232 $\tilde{A}_c^{(p)}$. Specifically, we approximate the powers Φ^m , which correspond to m applica-
 233 tions of the fine time integrator Φ , with a coarse operator Ψ . This results in the
 234 approximation $\tilde{A}_c^{(p)}$ given by

$$235 \quad \tilde{A}_c^{(p)} := \begin{bmatrix} I \\ -\Psi & I \\ \ddots & \ddots \\ -\Psi & I \end{bmatrix}_{\min(p+1,k)}.$$

236 Using this approximation, we can formulate the error-propagation \mathcal{E}_a using the ap-
 237 proximated local coarse-grid inverse. Again, we refer to [Appendix B](#) for derivations.
 238 The error-propagation operator with approximate coarse grid, \mathcal{E}_a , is then given by

$$239 \quad (3.3) \quad \mathcal{E}_a = \left[\begin{array}{cccccc} \overbrace{\mathbf{0} \cdots}^m & & & \overbrace{\mathbf{0}}^{m(N_T-1)} & & \overbrace{1}^1 \\ \mathcal{Z}_0 & \mathbf{0} & \cdots & & \mathbf{0} & \}^m \\ \vdots & \ddots & \ddots & \cdots & \mathbf{0} & \}^{(k-1)m} \\ \mathcal{Z}_{k-2} & \cdots & \mathcal{Z}_0 & \mathbf{0} & \cdots & \mathbf{0} \\ \mathcal{W} & \mathcal{Z}_{k-2} & \cdots & \mathcal{Z}_0 & \mathbf{0} & \cdots & \mathbf{0} \\ \mathbf{0} & \ddots & \ddots & \vdots & \ddots & \ddots & \vdots \\ \mathbf{0} & \ddots & \mathcal{W} & \mathcal{Z}_{k-2} & \cdots & \mathcal{Z}_0 & \mathbf{0} & \mathbf{0} \\ \mathbf{0} & \cdots & \mathbf{0} & \bar{\mathcal{W}} & \bar{\mathcal{Z}}_{k-2} & \cdots & \bar{\mathcal{Z}}_0 & \mathbf{0} \end{array} \right]_1,$$

240 with block matrices \mathcal{Z}_j and \mathcal{W} given by

$$241 \quad (3.4) \quad \mathcal{Z}_j = \left[\begin{array}{cccc} \overbrace{\Phi^0 \Psi^j (\Phi^m - \Psi)}^m & \mathbf{0} & \cdots & \mathbf{0} \\ \vdots & \vdots & \vdots & \vdots \\ \Phi^{m-1} \Psi^j (\Phi^m - \Psi) & \mathbf{0} & \cdots & \mathbf{0} \end{array} \right]_m \quad \mathcal{W} = \left[\begin{array}{cccc} \overbrace{\Phi^0 \Psi^{k-1} \Phi^m}^m & \mathbf{0} & \cdots & \mathbf{0} \\ \vdots & \vdots & \vdots & \vdots \\ \Phi^{m-1} \Psi^{k-1} \Phi^m & \mathbf{0} & \cdots & \mathbf{0} \end{array} \right]_m,$$

242 and $\bar{\mathcal{W}}$ and $\bar{\mathcal{Z}}_j$ are again identical to first row of \mathcal{W} and \mathcal{Z}_j , respectively.

243 **3.2. Convergence bounds.** To avoid multiple subscripts, we omit the subscript
244 a of \mathcal{E}_a from (3.3) in the sequel. Using f and c subscripts to denote F - and C -points,
245 respectively, \mathcal{E} (3.3) can be reordered and partitioned into 2×2 block form. Moreover,
246 notice that F -points columns of \mathcal{Z}_j and \mathcal{W} (3.4) (and therefore also of \mathcal{E}_a (3.3)) are all
247 zero. If we then consider powers of the matrix, which correspond to several iterations,
248 we get

$$249 \quad \mathcal{E}^\ell := \begin{bmatrix} \mathcal{E}_{ff} & \mathcal{E}_{fc} \\ \mathcal{E}_{cf} & \mathcal{E}_{cc} \end{bmatrix}^\ell = \begin{bmatrix} \mathbf{0} & \mathcal{E}_{fc} \\ \mathbf{0} & \mathcal{E}_{cc} \end{bmatrix}^\ell = \begin{bmatrix} \mathbf{0} & \mathcal{E}_{fc} \mathcal{E}_{cc}^{\ell-1} \\ \mathbf{0} & \mathcal{E}_{cc}^\ell \end{bmatrix}.$$

251 It follows from above that for multiple iterations, convergence is fully defined by
252 $\mathcal{E}_{cc} \in \mathbb{R}^{N_T+1 \times N_T+1}$, that is, \mathcal{E}^ℓ will be convergent in some norm, that is, $\|\mathcal{E}^\ell\| < 1$,
253 if and only if \mathcal{E}_{cc}^ℓ is as well. To that end, we consider analyzing the C-C principle
254 submatrix of (3.3),

255 (3.5) $\mathcal{E}_{cc} =$

$$256 \quad \left[\begin{array}{cccccc} \mathbf{0} & & & & & & \\ (\Phi^m - \Psi) & \mathbf{0} & & & & & \\ \vdots & (\Phi^m - \Psi) & \ddots & & & & \\ \Psi^{k-2}(\Phi^m - \Psi) & \vdots & \ddots & \mathbf{0} & & & \\ \Psi^{k-1}\Phi^m & \Psi^{k-2}(\Phi^m - \Psi) & \cdots & (\Phi^m - \Psi) & \mathbf{0} & & \\ \ddots & \ddots & \ddots & \vdots & \ddots & \ddots & \\ \Psi^{k-1}\Phi^m & \Psi^{k-2}(\Phi^m - \Psi) & \cdots & (\Phi^m - \Psi) & \mathbf{0} & & \end{array} \right].$$

257

258

259 Now consider the case of Φ and Ψ being simultaneously diagonalizable, as would
 260 occur if the same (diagonalizable) spatial matrix is used on the fine and coarse grid.
 261 Let U denote the shared eigenvector matrix of Φ and Ψ , with eigenvalues $\mu \in \sigma(\Psi)$
 262 and $\lambda \in \sigma(\Phi)$, where $\sigma(\Psi)$ and $\sigma(\Phi)$ denote the spectrum of Ψ and Φ , respectively.
 263 Following the frameworks developed in [9, 36], let \tilde{U} denote a block-diagonal matrix,
 264 with diagonal blocks given by eigenvectors U . Then,

$$265 \quad \|\mathcal{E}_{cc}\|_{(\tilde{U}\tilde{U}^*)^{-1}} = \max_{\{\mu, \lambda\}} \|\tilde{\mathcal{E}}_{cc}\|,$$

266 where $\|\cdot\|$ here corresponds to the ℓ^2 -norm, and $\tilde{\mathcal{E}}_{cc}$ is defined as follows for a fixed
 267 pair of eigenvalues $\{\mu, \lambda\}$:

$$268 \quad \tilde{\mathcal{E}}_{cc} :=$$

$$269 \quad \begin{bmatrix} \mathbf{0} & & & & & & \\ (\lambda^m - \mu) & \mathbf{0} & & & & & \\ \vdots & (\lambda^m - \mu) & \ddots & & & & \\ \mu^{k-2}(\lambda^m - \mu) & \vdots & \ddots & \mathbf{0} & & & \\ \mu^{k-1}\lambda^m & \mu^{k-2}(\lambda^m - \mu) & \dots & (\lambda^m - \mu) & \mathbf{0} & & \\ \ddots & \ddots & & \vdots & \ddots & \ddots & \\ & \mu^{k-1}\lambda^m & \mu^{k-2}(\lambda^m - \mu) & \dots & (\lambda^m - \mu) & \mathbf{0} & \end{bmatrix}.$$

271 If the spatial matrix is normal, then $(\tilde{U}\tilde{U}^*)^{-1} = I$. In general, bounding $\tilde{\mathcal{E}}_{cc}$ in the
 272 ℓ^2 -norm for each eigenvalue pair guarantees convergence of \mathcal{E}_{cc} in a certain eigenvector
 273 induced norm, where “convergence” corresponds to a guaranteed reduction in error
 274 every iteration (in contrast to, e. g., nilpotency, where convergence is eventually guar-
 275 anteed, but error could in principle diverge significantly for many iterations before
 276 sudden convergence to the exact solution).

277 Recall the inequality $\|\tilde{\mathcal{E}}_{cc}\|^2 \leq \|\tilde{\mathcal{E}}_{cc}\|_1 \|\tilde{\mathcal{E}}_{cc}\|_\infty$. Given that $\tilde{\mathcal{E}}_{cc}$ is Toeplitz, the
 278 maximum row and column sums are equal, yielding the bound

$$279 \quad \|\tilde{\mathcal{E}}_{cc}\| \leq \|\tilde{\mathcal{E}}_{cc}\|_1 = |\lambda^m - \mu| \sum_{\ell=0}^{k-2} |\mu^\ell| + |\lambda^m \mu^{k-1}|$$

$$280 \quad (3.6) \quad = \frac{|\lambda^m - \mu|(1 - |\mu|^{k-1})}{1 - |\mu|} + |\lambda^m \mu^{k-1}|.$$

282 Results are summarized in the following theorem.

283 **THEOREM 3.1** (Two-level convergence). *Let Φ and Ψ be simultaneously diag-
 284 onalizable with eigenvectors U , and consider two-level AT-MGRIT with coarsening
 285 factor m and local coarse-grid size k . For a given CF-splitting of time points, error
 286 propagation takes the form*

$$287 \quad \mathcal{E}^\ell := \begin{bmatrix} \mathcal{E}_{ff} & \mathcal{E}_{fc} \\ \mathcal{E}_{cf} & \mathcal{E}_{cc} \end{bmatrix}^\ell = \begin{bmatrix} \mathbf{0} & \mathcal{E}_{fc} \mathcal{E}_{cc}^{\ell-1} \\ \mathbf{0} & \mathcal{E}_{cc}^\ell \end{bmatrix}.$$

289 *Further, assume Φ and Ψ are stable in an eigenvalue sense, that is, $|\mu|, |\lambda| < 1$ for
290 all $\mu \in \sigma(\Psi)$, $\lambda \in \sigma(\Phi)$, and define*

$$291 \quad \varphi_{tg}(\mu, \lambda) := \frac{|\lambda^m - \mu|}{1 - |\mu|}$$

292 *for eigenvalue pairs (with shared eigenvector) $\{\mu, \lambda\}$. Then,*

$$293 \quad (3.7) \quad \|\mathcal{E}_{cc}\|_{(\tilde{U}\tilde{U}^*)^{-1}} \leq \max_{\{\mu, \lambda\}} (\varphi_{tg}(\mu, \lambda) + |\mu^{k-1}| (|\lambda^m| - \varphi_{tg}(\mu, \lambda))).$$

295 *Proof.* The proof follows from a simple expansion of (3.6). \square

296 **COROLLARY 3.2.** *Under the same assumptions as Theorem 3.1,*

$$297 \quad (3.8) \quad \|\mathcal{E}_{cc}\|_{(\tilde{U}\tilde{U}^*)^{-1}} \leq \max_{\{\mu, \lambda\}} (\varphi_{tg}(\mu, \lambda) + |\mu^k| (1 - \varphi_{tg}(\mu, \lambda))).$$

299 *Proof.* Note that

$$300 \quad \frac{|\lambda^m - \mu|(1 - |\mu|^{k-1})}{1 - |\mu|} = \frac{|\lambda^m - \mu|(1 - |\mu|^k)}{1 - |\mu|} - |\mu^{k-1}| |\lambda^m - \mu|$$

302 In addition, we have $|\lambda^m \mu^{k-1}| = |\mu^{k-1}(\lambda^m - \mu) + \mu^k| \leq |\mu^{k-1}| |\lambda^m - \mu| + |\mu^k|$. Plugging
303 these two results into (3.6), yields an upper bound

$$304 \quad \|\mathcal{E}_{cc}\|_{(\tilde{U}\tilde{U}^*)^{-1}} \leq \max_{\{\mu, \lambda\}} \left(\frac{|\lambda^m - \mu|(1 - |\mu|^k)}{1 - |\mu|} + |\mu^k| \right).$$

305 An analogous expansion as used in Theorem 3.1 completes the proof. \square

306 Note that the first term, φ_{tg} , in (3.7) and (3.8), to $\mathcal{O}(1/N_T)$, provides necessary
307 and sufficient conditions for convergence of two-level Parareal and MGRIT [9, 36, 37],
308 while the second term introduces an error perturbation that results from truncating
309 the coarse grid. Although Corollary 3.2 is less tight than Theorem 3.1, it provides
310 a more intuitive description of convergence. Note that error modes which converge
311 fast for traditional Parareal/MGRIT, $\varphi_{tg}(\mu, \lambda) \approx 0$, lead to the largest perturbation
312 of convergence for AT-MGRIT, $\approx |\mu^k|$ (this also suggests convergence will be better
313 for a more “diffusive” coarse solver, that is, a coarse solver with generally smaller
314 eigenvalues). In contrast, there will be much less degradation in convergence for
315 modes that are relatively slow to converge for traditional Parareal/MGRIT.

316 This leads to a further important observation on convergence of AT-MGRIT : with
317 some algebra,¹ one can show that the “error” subdiagonal, that is, the subdiagonal
318 of $\tilde{\mathcal{E}}_{cc}$ that lacks a $\lambda^m - \mu$ scaling, is propagated out of the matrix after $\lceil (N_T + 1)/k \rceil$
319 iterations (i.e., all matrix entries then have at least one power of $\lambda^m - \mu$). This
320 suggests a natural heuristic to choose k :

321 **Choice of k :** choose k at least large enough so that $\lceil (N_T + 1)/k \rceil$ approximates the
322 number of iterations to converge for traditional two-level Parareal.

¹There are various ways to show this; perhaps the most formal is in noting that multiplication of Toeplitz matrices such as $\tilde{\mathcal{E}}_{cc}^\ell$ corresponds to finite discrete convolutions. One can also simply expand $\tilde{\mathcal{E}}_{cc}^p = (\tilde{\mathcal{E}}_{cc} + \mu^{k-1} \lambda^m I_{-k})^p$, where I_{-k} is a diagonal of ones on the k th subdiagonal.

323 The number of iterations for Parareal convergence is defined by the slowest converging
 324 modes, which are in turn the least affected in convergence of AT-MGRIT by the
 325 perturbation term in (3.7) and (3.8) (i.e., we expect these modes to converge in a
 326 roughly similar number of iterations for AT-MGRIT). As mentioned previously, the
 327 fastest-converging modes for Parareal/MGRIT, however, can suffer significant degra-
 328 dation of convergence in AT-MGRIT. Thus, we choose k so that the error perturbation
 329 for these terms is eliminated via nilpotency at (approximately) the same number of
 330 iterations as the slowest converging modes for standard Parareal/MGRIT will have
 331 converged. After this nilpotency is achieved, these “fast” modes will rapidly converge
 332 (if they have not already) due to $\varphi_{tg}(\mu, \lambda) \ll 1$. These observations can be seen in
 333 practice in [Figure 6\(b\)](#), where at almost exactly $\lceil (N_T + 1)/k \rceil$ iterations, the residual
 334 drops precipitously, decreasing by as much as four orders of magnitude on the fol-
 335 lowing iteration (see [Figures 6\(a\)](#) and [6\(b\)](#) and surrounding text for a more detailed
 336 discussion).

337 Last, it is important to remember that theory developed in this section is for two-
 338 level AT-MGRIT applied to linear problems. The resulting heuristic for choosing k
 339 provides a good starting point, but multilevel AT-MGRIT or application to nonlinear
 340 problems as considered in [Section 5](#) may require larger k (e.g., see [Table 4](#)).

341 **4. Algorithmic properties.** This section examines nuances of the AT-MGRIT
 342 algorithm, including a communication scheme for distributing residuals on the coarsest
 343 level ([Subsection 4.1](#)), the implicit propagation of initial conditions across the time
 344 domain ([Subsection 4.2](#)), and a study on the new parameter k ([Subsection 4.3](#)).

345 **4.1. Implementation.** We have implemented [Algorithm 2.2](#) in parallel as part
 346 of the PyMGRIT package [\[19, 4\]](#) framework. When applying the algorithm in parallel,
 347 we assume that at the coarsest level at most one C -point of the global grid lies on
 348 one process. In principle this is not necessary, but ensures that the solves of the local
 349 problems can be perfectly parallelized. To solve the local problems, the fine(r)-level
 350 residuals must be distributed. Let p_0, p_1, \dots, p_{N_T} , where N_T is equal to the number
 351 of points on the coarsest global coarse grid, be all processes containing a C -point
 352 on the coarsest grid. Then, we define two groups of MPI communicators. The first
 353 decomposition divides all processes based on the local grid size k into $\lceil (N_T + 1)/k \rceil$
 354 groups, where the first group consists of processes p_0, p_1, \dots, p_{k-1} , the second consists
 355 of processes $p_k, p_{k+1}, \dots, p_{2k-1}$, and so on. The second decomposition divides the
 356 processes p_{k-1}, \dots, p_{N_T} into groups of size k , so that the first group consists of processes
 357 p_{k-1}, \dots, p_{2k-2} , the next of processes $p_{2k-1}, \dots, p_{3k-1}$, and so on. Then, the distribution
 358 of residuals is given by a communication within all groups of the first decomposition,
 359 followed by a communication within all groups of the second decomposition. Note that
 360 the groups of a decomposition do not overlap, allowing for parallel communication
 361 within each group. [Figure 3](#) shows an example of the residual communication for a
 362 two-level AT-MGRIT algorithm with a global coarse grid with $N_T = 5$, along with a
 363 description of the communication stages.

364 **4.2. Propagation of the initial condition.** A key feature of the AT-MGRIT
 365 algorithm is the implicit propagation of the initial condition through the iterations
 366 of the method, which allows for using local coarse grids that do not include the
 367 initial time point. The idea of implicit propagation of the initial condition is best
 368 explained in a two-level example with F -relaxation. [Figure 4](#) shows an example of
 369 the distribution of local coarse grids for $N_t = 20$, $m = 7$ and $k = 3$. Only the first
 370 three local coarse grids have direct access to the initial condition and, thus, the initial

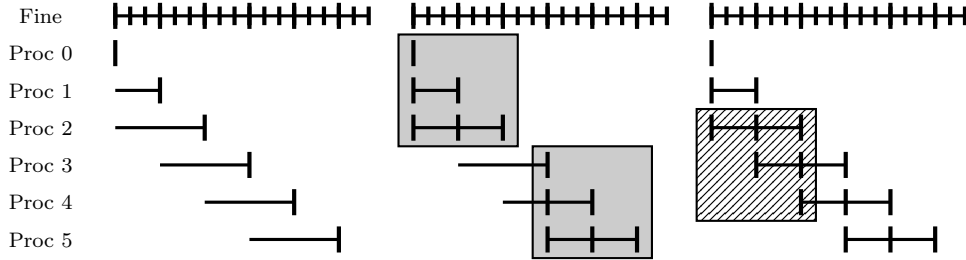


Fig. 3: Illustration of the communication scheme for $P = 6$ processes and local grid size $k = 3$. First (left), each process computes the residual of its rightmost C -point. In a second step (middle), the residuals are distributed in parallel within the groups of the first decomposition (gray boxes). Last (right), the residuals are distributed within the groups of the second decomposition (shaded boxes), after which each process has all the required residuals.

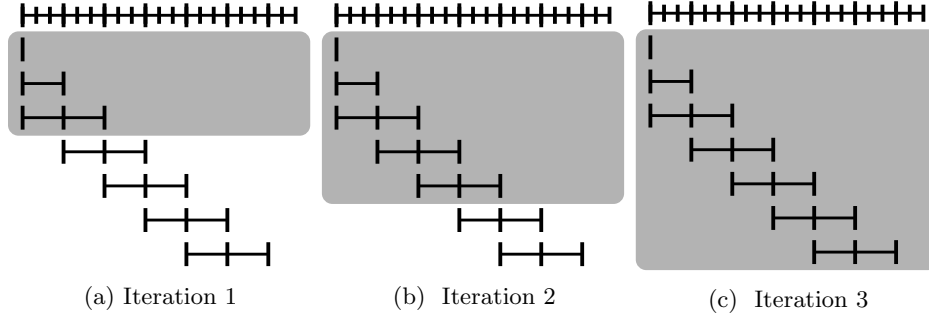


Fig. 4: Implicit propagation (gray box) of the initial condition for a two-level AT-MGRIT variant with F -relaxation and $N_t = 20$, $m = 3$ and $k = 3$.

371 condition is distributed over the first three local coarse grids in the first iteration. All
 372 other local coarse grids do not have access to the initial condition at this point. In
 373 the second iteration, again only the first three local coarse grids directly contain the
 374 initial condition. However, the next two local coarse grids now contain C -points of
 375 local coarse grids, which directly depend on the initial condition from the previous
 376 iteration, making them implicitly depend on the initial condition as well. In the next
 377 iteration, the next two local coarse grids implicitly depend on the initial condition,
 378 and so on. In the end, the two-level AT-MGRIT algorithm with F -relaxation requires
 379 $\lceil (N_t + 1)/k \rceil$ iterations until all local coarse grids depend implicitly on the initial
 380 condition. Note that in the two-level variant with FCF -relaxation, the initial value
 381 is also propagated to the next C -point on the fine grid due to the additional CF -
 382 relaxation and, thus, the initial condition is propagated faster. Also note that the
 383 propagation in the multi-level case is even faster than in the two-level case, since the
 384 initial condition is additionally propagated by the relaxations on the intermediate
 385 level(s).

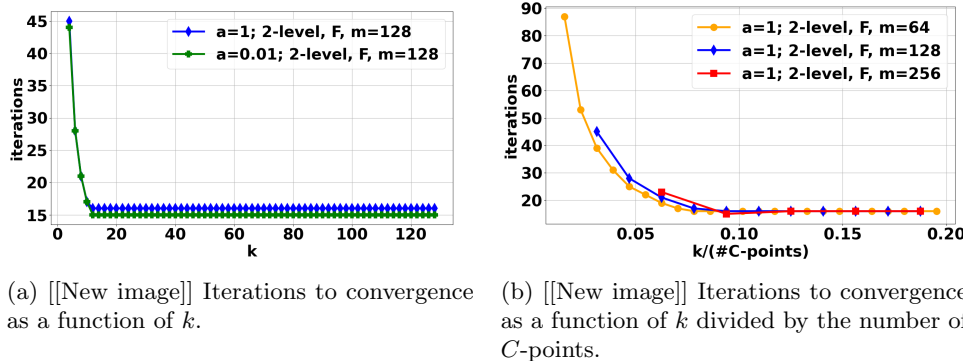
386 **4.3. Size of local coarse grids.** The parameter k defines the size of the local
 387 coarse grids and, thus, the number of sequential solves needed on the coarse grid.
 388 In the following, we consider the influence of the parameter k on the convergence of
 389 AT-MGRIT applied to a standard model problem for parallel-in-time methods, the
 390 one-dimensional heat equation,

391 (4.1)
$$u_t - au_{xx} = b(x, t) \quad \text{in } [0, 3] \times [0, \pi],$$

392 where a is the thermal conductivity, and subject to the initial condition $u(x, 0) =$
 393 $\sin(\pi x)$ and homogeneous Dirichlet boundary conditions in space. The forcing term
 394 is chosen as $b(x, t) = -\sin(\pi x)(\sin(t) - \pi^2 \cos(t))$, such that the exact solution is
 395 given by $u(x, t) = \sin(\pi x) \cos(t)$ for $a = 1$. We first examine the behavior of k for
 396 $a = 1$ and $a = 0.01$, and then choose $a = 1$ for more detailed results.

397 We discretize (4.1) using second-order central finite differences with 1,025 degrees
 398 of freedom in space and on an equidistant time grid with 16,384 time points using
 399 backward Euler. We investigate the behavior of the AT-MGRIT algorithm for the
 400 two-level case, and choose different coarsening factors m and local grid sizes k . We
 401 restrict ourselves to the two-level case, since we want to study the effect of using local
 402 coarse grids of various sizes k . For all simulations, the stopping tolerance is based on
 403 the discrete 2-norm of the absolute space-time residual with a tolerance of 10^{-7} and a
 404 random initial guess is chosen for all time points except for the initial condition. This
 405 choice guarantees that no knowledge of the right-hand side is used that could affect
 406 the convergence. Note that this is only a good choice for investigating the behavior
 407 of the algorithm and is not recommended in practice.

408 Figure 5(a) shows the required number of iterations to reach the stopping criterion
 409 for a two-level AT-MGRIT variant with F -relaxation and a coarsening factor of $m =$
 410 128 as a function of size k for the two choices of the thermal conductivity. Note
 411 that while the variant with $k = 128$, which is equivalent to Parareal, performs 127
 412 sequential time steps on the coarse level, equivalent convergence can be obtained
 413 with $k = 12$, 10× less coarse-grid solves. Note, that the behavior is similar for both
 414 choices of a . Figure 5(b) presents iterations to convergence as a function of the ratio
 415 of local to global coarse-grid points. For three different coarsening factors, we see
 416 that convergence does not improve beyond the same ratio of $k/(\#C\text{-points})$, in this
 417 case about 0.08. Although this parameter is likely problem specific, Figure 5(b) does
 418 suggest the choice of k is relatively agnostic to that of the coarsening factor by posing
 419 it relative to the global coarse-grid size.

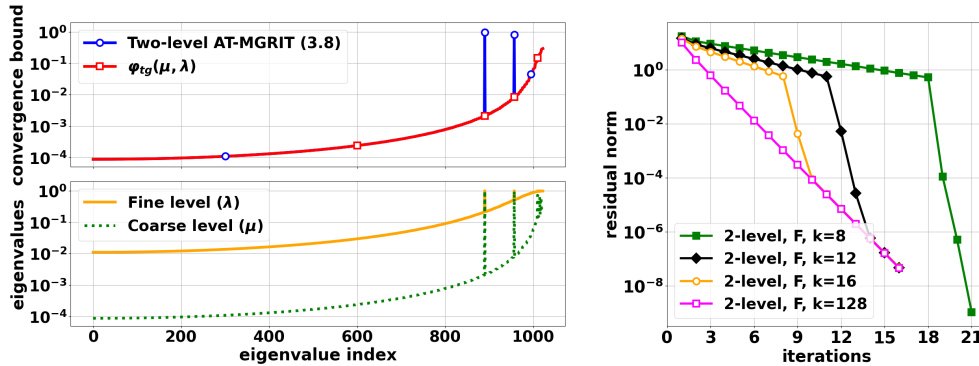


(a) [[New image]] Iterations to convergence as a function of k .

(b) [[New image]] Iterations to convergence as a function of k divided by the number of C -points.

Fig. 5: Required iterations for AT-MGRIT variants for the 1D heat equation.

420 To better understand the convergence behavior described in [Subsection 3.2](#), for
 421 each spatial eigenvalue [Figure 6\(a\)](#) plots the theoretical convergence rate [\(3.8\)](#), the
 422 (asymptotic in N_T) two-grid rate φ_{tg} , and the corresponding eigenvalues for the
 423 coarse- and fine-propagator for two-level AT-MGRIT with $m = 128$ and $k = 12$.
 424 Notice that on an eigenvector basis, theoretical convergence of AT-MGRIT almost
 425 exactly matches that of Parareal, with (in this case) two exceptions, given by the
 426 blue dots with convergence ≈ 1 . Each of these spatial eigenmodes correspond with
 427 a coarse-propagator eigenvalue $|\mu| \approx 1$ and $\varphi_{tg} \ll 1$, which (see [Corollary 3.2](#)) leads
 428 to a significant degradation in convergence (in a single-iteration sense). [Figure 6\(b\)](#)
 429 plots *observed* convergence behavior for two-level AT-MGRIT with coarsening factor
 430 $m = 128$ and various choices for k . The variant with $k = 128$ (i.e., Parareal) has
 431 uniform convergence behavior, while convergence for smaller k is split into three parts.
 432 Initially, convergence is much slower than for $k = 128$, due to the spatial eigenmodes
 433 with $|\mu^k| \approx 1$ and $\varphi_{tg} \ll 1$ discussed above. The smaller k is chosen, the slower is
 434 the convergence, since the convergence perturbation of $|\mu^k|(1 - \varphi_{tg})$ in [Corollary 3.2](#)
 435 decreases with increased k . However, after almost exactly $(N_T + 1)/k$ iterations (see
 436 [Theorem 3.1](#) and surrounding discussion), once the initial condition has been implicity
 437 propagated over all local coarse grids, these problematic modes are eliminated
 438 via nilpotency and a drastic improvement in convergence can be seen for all three
 439 variants; e.g., for $k = 8$, one iteration suddenly reduces the residual norm almost four
 440 orders of magnitude. This rapid convergence lasts until the residual norm matches
 441 that of Parareal, and convergence rates thereafter follow Parareal. Comparing the
 442 theoretical and numerical results for $m = 12$, the theoretical bound (see [Figure 6\(a\)](#))
 443 is given by 0.94987 and the maximum numerical convergence factor between two iter-
 444 ations for the equivalent setting (see [Figure 6\(b\)](#)) is given by 0.7418. Note, observed
 445 convergence is better than the theoretical bound due to many modes being rapidly
 446 attenuated. Only a few modes are very slow to converge, with rates likely close to
 447 the theoretical bound, but these modes degrade the average (across all error modes)
 448 convergence rate.



(a) Theoretical bound on convergence rate based on [\(3.8\)](#), φ_{tg} , and eigenvalues sorted by φ_{tg} , for $m = 128$ and $k = 12$.

(b) Residual norm as a function of iteration for two-level AT-MGRIT with coarsening factor $m = 128$.

Fig. 6: Results of AT-MGRIT variants in terms of theoretical error bound [\(3.8\)](#) and residual norm for the heat equation with $a = 1$.

449 **5. Parallel results.** In this section, we present numerical results for AT-MGRIT
 450 applied to two challenging, nonlinear time-dependent problems: the 2D Gray Scott
 451 example of a chemical reaction of two substances, and a realistic model of an electrical
 452 machine. In addition, we apply different two- and three-level variants of AT-MGRIT
 453 and compare runtimes and iteration counts with the corresponding variants of Parareal
 454 and MGRIT, respectively. For the two-level variants, we apply F -relaxation and we
 455 choose the coarsening factor such that the number of coarse-grid points is equal to the
 456 number of processes used for the simulation enabling perfect parallelization on the
 457 fine level. For the three-level algorithms, we apply non-uniform coarsening strategies
 458 with a coarsening factor of $m_0 = 64$ between the fine and the intermediate level, and
 459 different factors between the intermediate and the coarse level. All simulations
 460 were performed on an Intel Xeon Phi Cluster consisting of four 1.4 GHz Intel Xeon
 461 Phi processors. The code for all experiments can be found in the PyMGRIT repository
 462 [18], and this package is also used for simulations with Parareal and MGRIT. For all
 463 experiments, we use all possible resources for temporal parallelization, i. e., we do not
 464 use spatial parallelization (largely due to limited resources). For a brief discussion on
 465 the effect of spatial parallelism for the different algorithms, see [Appendix C](#).

466 **5.1. Gray Scott.** We consider the 2D Gray-Scott problem [32] of a chemical
 467 reaction of two components \mathcal{U} and \mathcal{V} , given by

$$468 \quad u_t = D_u \Delta u - uv^2 + F(1 - u), \\ 469 \quad v_t = D_v \Delta v + uv^2 - (K + F)u,$$

471 where $u = u(x, y, t)$ and $v = v(x, y, t)$ are the concentration of \mathcal{U} and \mathcal{V} , respectively,
 472 D_u and D_v are the diffusion rates, F is the feed rate, and K is the removal rate. For our
 473 simulations, we choose the spatial domain $[0, 2.5]^2$ with periodic boundary conditions,
 474 and the time interval $[0, 256]$. Further, we choose the parameters $F = 0.024$, $K = 0.06$,
 475 $D_u = 8 \times 10^{-5}$, and $D_v = 4 \times 10^{-5}$, and we consider the initial value

$$476 \quad u(x, y, 0) = 1 - 2(0.25 \sin(4\pi x)^2 \sin(4\pi y)^2), \quad (x, y) \in [1, 1.5]^2 \\ 477 \quad v(x, y, 0) = 0.25 \sin(4\pi x)^2 \sin(4\pi y)^2, \quad (x, y) \in [1, 1.5]^2,$$

479 and $u(x, y, 0) = 1$ and $v(x, y, 0) = 0$ otherwise. The problem is discretized using
 480 central finite differences with 128^2 points in space and on an equidistant time grid
 481 with 16,384 points using backward Euler. We solve the resulting nonlinear problem
 482 using Newton's method of PETSc [1] with a relative and absolute tolerance of 10^{-10} .

483 We apply two-level and three-level AT-MGRIT variants, and compare the two-
 484 level variants with Parareal variants and the three-level variants with MGRIT. Fur-
 485 thermore, we use nested iterations to compute an improved initial guess. In the nested
 486 iteration strategy, Parareal and MGRIT solve the global coarse-grid problem at the
 487 coarsest level, while AT-MGRIT uses the local coarse grids instead of the global grid.
 488 The stopping criterion for all variants is based on the discrete 2-norm of the space-time
 489 residual with a tolerance of 10^{-7} .

490 Table 1 shows the number of iterations and runtimes of the setup and solve phases
 491 of two-level AT-MGRIT and Parareal variants. The setup time consists of comput-
 492 ing an improved initial guess and the solve time consists of applying the algorithm.
 493 The results show that iteration counts of AT-MGRIT are equal to iteration counts of
 494 Parareal with the same coarsening strategy. Furthermore, a finer coarse grid signifi-
 495 cantly reduces the number of iterations required. While 12 iterations are needed for
 496 the two-level variants with a coarse grid of only 32 points, this number is reduced to

Method	m	k	# Procs	# Iters	Setup time	Solve time	Speedup w.r.t Parareal
Parareal	512	-	32	12	1,338 s	172,068 s	-
	256	-	64	10	2,308 s	89,288 s	-
	128	-	128	9	3,958 s	66,485 s	-
	64	-	256	7	7,646 s	66,272 s	-
Two-level AT-MGRIT	512	16	32	12	701 s	165,351 s	1.04
	256	32	64	10	1,167 s	78,230 s	1.15
	128	64	128	9	2,022 s	48,675 s	1.39
	64	128	256	7	3,812 s	39,895 s	1.69

Table 1: Iteration counts, setup times (for computing an improved initial guess), and runtimes of the solve phase of two-level AT-MGRIT and Parareal variants applied to the 2D Gray-Scott problem for various numbers of processes.

497 seven iterations for the variants with 256 coarse-grid points. However, this reduction
 498 in iterations is accompanied by significantly more expensive sequential coarse-grid
 499 solves, reflected in increasing setup times with increasing points on the coarse grid.
 500 However, if the number of points on the coarse grid doubles, the setup time does not
 501 double. This is because a smaller time step requires fewer Newton iterations and,
 502 thus, affects the duration of the application of each time integration. The setup time
 503 of each AT-MGRIT variant is about half as long as that of the corresponding Parareal
 504 variant due to the choice of k . Looking at the runtimes of the solve phase, we see
 505 that AT-MGRIT is always faster than the corresponding Parareal variant, achieving
 506 a speedup of up to a factor of 1.69 compared to Parareal. Furthermore, we see that
 507 while the Parareal algorithm does not scale for more than 128 processes, since the se-
 508 rial part of the algorithm dominates the benefit of the additional parallelization of the
 509 fine level, the AT-MGRIT algorithm shows good parallel scaling up to 256 processes.
 510

511 **Table 2** presents similar results to **Table 1** for four different three-level variants
 512 of AT-MGRIT and MGRIT with *FCF*-relaxation on 256 processes. The number of
 513 iterations here does not depend as much on the coarsest grid as in the two-level case,
 514 but we still see that the MGRIT variant with the coarsening strategy (64, 2), i. e., the
 515 variant with the most points on the second level, requires the fewest iterations. The
 516 corresponding AT-MGRIT variant needs one additional iteration, but after the sixth
 517 iteration the stopping criterion is slightly missed. A minimal increase in k would likely
 518 eliminate this extra iteration. In terms of solve times, we see that all variants of the
 519 AT-MGRIT algorithm are faster than the corresponding MGRIT variants, even the
 520 variant that requires an additional iteration. Again, the more points on the coarsest
 521 level, the higher the speedup of AT-MGRIT over MGRIT. Note that for this problem,
 522 adding a coarser level to the three-level MGRIT variants does not guarantee further
 523 reduction of the runtime. Rather, adding a level may increase the runtime. For
 524 example, the four-level MGRIT with the coarsening strategy (64, 8, 2), which adds

Method	m	k	# Iters	Setup time	Solve time	Speedup w.r.t MGRIT
MGRIT	(64,16)	-	7	3,525 s	43,604 s	-
	(64,8)	-	7	3,498 s	38,420 s	-
	(64,4)	-	7	4,980 s	42,285 s	-
	(64,2)	-	6	8,075 s	45,131 s	-
AT-MGRIT	(64,16)	8	7	2,864 s	41,054 s	1.07
	(64,8)	16	7	2,174 s	33,688 s	1.17
	(64,4)	32	7	2,713 s	34,063 s	1.29
	(64,2)	64	7	4,247 s	38,571 s	1.24

Table 2: Iteration counts and runtimes of the setup and solve phase on 256 processes of three-level AT-MGRIT and MGRIT variants with *FCF*-relaxation and different non-uniform coarsening strategies applied to the 2D Gray-Scott problem.

Method	m	k	# Iters	Setup time	Solve time	Speedup w.r.t MGRIT
AT-MGRIT	(64,8)	4	10	1,140 s	42,063 s	0.97
	(64,8)	6	9	1,357 s	38,978 s	1.04
	(64,8)	8	8	1,543 s	35,767 s	1.12
	(64,8)	10	8	1,716 s	36,509 s	1.10
	(64,8)	12	8	1,877 s	37,060 s	1.08
	(64,8)	14	8	2,047 s	37,786 s	1.05
	(64,8)	16	7	2,174 s	33,688 s	1.17

Table 3: Iteration counts and runtimes of the setup and solve phase on 256 processes of three-level AT-MGRIT with *FCF*-relaxation, coarsening factor (64, 8), and different choices of k applied to the 2D Gray-Scott problem.

525 another level with a coarsening factor of two to the variant with the coarsening factor
 526 (64, 8) from Table 2, requires eight iterations and the overall runtime (setup and solve)
 527 is 52,370 s.

528 Table 3 extends the results from Table 2 and shows the effect of different choices
 529 of k for the three-level AT-MGRIT with coarsening factor (64, 8). We see that the
 530 number of iterations increases slightly as k decreases. Despite the increasing number
 531 of iterations, the runtime for all $k \geq 6$ is smaller than the runtime of the corresponding
 532 MGRIT variant from Table 2. For smaller k , the runtime is larger compared to the
 533 MGRIT variant because the cost of the additional iterations is more expensive than
 534 the cost reduction due to the local coarse grids.

535 Figure 7 shows the overall runtime for one AT-MGRIT variant (blue line) and the
 536 corresponding MGRIT variant (orange line) as a function of the number of processes

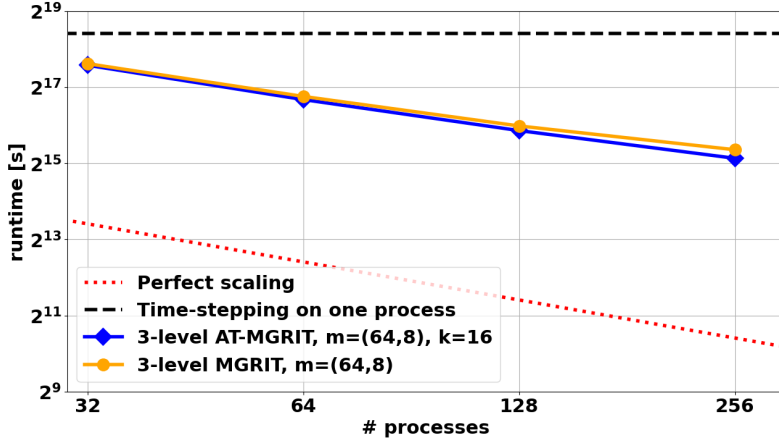


Fig. 7: Strong scaling results for one three-level AT-MGRIT variant, the corresponding MGRIT variant, and sequential time-stepping on one process applied to the 2D Gray-Scott problem. The red dotted line indicates the perfect scaling based on the runtime of time-stepping.

537 and the runtime of time-stepping using only one process (black dashed line) which is
 538 about four days. For reference, the red dotted line indicates the behavior of perfect
 539 scaling based on the runtime of time-stepping. While the runtime almost halves when
 540 using 32 and 64 processes, the scaling curve starts to flatten slightly with a higher
 541 number of processes. This is mainly because only the fine level computations have an
 542 additional benefit from more processes due to the chosen coarsening strategy, and the
 543 runtime of the coarser levels becomes more and more dominant. However, compared
 544 to the corresponding MGRIT variant, the AT-MGRIT variant scales better due to its
 545 reduced work at the coarsest level.

546 **5.2. Induction machine.** The standard approach for the simulation of elec-
 547 trical machines is based on neglecting the displacement current in Maxwell's equa-
 548 tions [21]. The resulting magnetoquasistatic approximation, the so-called eddy cur-
 549 rent problem, is defined in terms of the unknown magnetic vector potential $\mathbf{A} :
 550 \Omega \times (t_0, t_f] \rightarrow \mathbb{R}^3$ as

$$551 \quad \sigma \partial_t \mathbf{A} + \nabla \times (\nu(\cdot) \nabla \times \mathbf{A}) = \mathbf{J}_s \text{ in } \Omega \times (t_0, t_f],$$

$$552 \quad \mathbf{n} \times \mathbf{A} = 0 \text{ on } \partial\Omega,$$

554 with initial value $\mathbf{A}(\mathbf{x}, t_0) = \mathbf{A}_0(\mathbf{x})$, spatial domain Ω , consisting of the rotor, stator,
 555 and the air gap in between, and where $(t_0, t_f]$ is the time interval. The magnetic flux
 556 $\mathbf{B} = \nabla \times \mathbf{A}$ vanishes at the boundaries $\partial\Omega$ of the spatial domain (Dirichlet boundary
 557 condition). Three ($n_s = 3$) distributed stranded conductors are modeled by the source
 558 current density $\mathbf{J}_s = \sum_{s=1}^{n_s} \chi_s i_s$, with winding functions $\chi_s : \Omega \rightarrow \mathbb{R}^3$ and currents
 559 $i_s : (t_0, t_f] \rightarrow \mathbb{R}^3$. An attached electrical network provides a connection between the
 560 so-called flux-linkage, i. e., the spatially integrated time derivative of the magnetic
 561 vector potential, and the voltage. The scalar electrical conductivity $\sigma(\mathbf{x}) \geq 0$ and the
 562 (nonlinear) magnetic reluctivity $\nu(\mathbf{x}, |\nabla \times \mathbf{A}|) > 0$ encode the geometry. To consider
 563 the rotation of the rotor, the problem is extended by an additional equation of motion;
 564 we refer to [4] for more details.

565 In the following, we consider a cross-section in the x, y -plane to reduce the spatial
 566 domain to a two-dimensional (2D) domain $\Omega_{2D} \subset \mathbb{R}^2$. Discretizing in space using
 567 finite elements with n_a degrees of freedom yields a system of differential-algebraic
 568 equations of the form

569 (5.4a)
$$M\mathbf{u}'(t) + K(\mathbf{u}(t))\mathbf{u}(t) = \mathbf{f}(t), \quad t \in (t_0, t_f]$$

570 (5.4b)
$$\mathbf{u}(t_0) = \mathbf{u}_0,$$

572 with unknown $\mathbf{u}^\top = [\mathbf{a}^\top, \mathbf{i}^\top, \theta, \omega] : (t_0, t_f] \rightarrow \mathbb{R}^n$. At each point in time $t \in (t_0, t_f]$, the
 573 solution $\mathbf{u}(t) \in \mathbb{R}^n$ consists of the magnetic vector potentials $\mathbf{a}(t) \in \mathbb{R}^{n_a}$, the currents
 574 of the three phases $\mathbf{i}(t) \in \mathbb{R}^3$, the rotor angle $\theta(t) \in \mathbb{R}$, and the angular velocity of the
 575 rotor $\omega(t) \in \mathbb{R}$. The given voltages $\mathbf{v}(t) \in \mathbb{R}^3$ and the mechanical excitation define
 576 the right-hand side $\mathbf{f}(t)$. Note, that (5.4) is a differential-algebraic equation of index-1
 577 [3, 7] due to the presence of non-conducting materials, i.e., regions with $\sigma = 0$, in
 578 the domain, which can be treated by standard techniques in a parallel-in-time setting
 579 [35].

580 The multi-slice finite element model “im_3.kw” [17] of a four-pole squirrel cage
 581 induction machine is used for modeling the semi-discrete problem (5.4). A mesh
 582 representation with $n_a = 4449$ degrees of freedom is generated using Gmsh [15, 16].
 583 Further, we choose $t_0 = 0$, $t_f = 0.2$ and a time grid with $N_t = 16,384$ points, which
 584 corresponds to a time-step size of $\delta t \approx 10^{-5}$. Note that this time interval is required
 585 approximately to reach the steady-state of the machine. For the simulations, only a
 586 quarter of the machine is considered with periodic boundary conditions and the **GetDP**
 587 library [10, 14], which implements the time integration using backward Euler, is used
 588 for the computations. At each time step, the **GetDP** library is called and a nonlinear
 589 problem is solved by applying Newton’s method with damping. For the stopping
 590 criterion of the Newton solver, we choose a relative error of 10^{-6} . The machine is
 591 supplied by a three-phase sinusoidal voltage source, and, as proposed in [17], an initial
 592 ramp-up of the applied voltage is used for reducing the transient behavior of the motor
 593 for the time interval $[0, 0.04]$.

594 In the following, we present results for one Parareal variant and several two-level
 595 AT-MGRIT variants. For all experiments, we use an improved initial guess given by
 596 a global coarse-grid solve. Unfortunately, the use of too large time steps on the coarse
 597 level in the simulation of the electrical machine in the time-parallel setting causes
 598 at least one nonlinear solve within **GetDP** to fail to converge. Note that this also
 599 prevents the use of another, even coarser level. To overcome this problem, we apply
 600 subcycling at the coarse level, i.e., we apply three smaller steps per time step at the
 601 coarse level, reducing the time step size and improving the accuracy of the solution.
 602 For all algorithms, we use a convergence criterion based on the relative change in
 603 Joule losses, an important quantity of an electrical machine, at all C -points of two
 604 successive iterations; see [4] for details. The algorithm terminates when the maximum
 605 norm of the relative difference of two successive iterations is less than 1%. Note that
 606 this criterion does not guarantee convergence to the discrete time-stepping solution,
 607 but for each variant it has been verified that it does indeed iterate to the discrete
 608 time-stepping solution.

609 Table 4 shows the number of iterations, total runtimes, and the speedup com-
 610 pared to sequential time-stepping on one process for different AT-MGRIT variants
 611 and Parareal. Furthermore, the speedup compared to Parareal is shown for all AT-
 612 MGRIT variants. Comparing the number of iterations, the Parareal algorithm and
 613 AT-MGRIT with $k = 24$ both require five iterations to convergence. For $16 \geq k \geq 22$,

Method	k	Iterations	Total time (Setup + Solve)	Speedup w.r.t Parareal	Speedup w.r.t time-stepping on one process
Parareal	-	5	40,544 s	-	4.64
Two-level AT-MGRIT	12	8	39,480 s	1.03	4.77
	14	7	36,188 s	1.12	5.2
	16	6	32,710 s	1.24	5.75
	18	6	33,337 s	1.22	5.64
	20	6	33,996 s	1.19	5.53
	22	6	34,626 s	1.17	5.43
	24	5	30,582 s	1.33	6.15

Table 4: Iteration counts and total runtimes on 64 processes of Parareal and various two-level AT-MGRIT variants with a coarsening factor of 256 for the simulation of the induction machine.

614 six iterations are needed to reach the stopping criterion, and for $k = 14$ and $k = 16$,
 615 seven and eight iterations, respectively. Despite the increased number of iterations
 616 for some variants, the total runtime of all AT-MGRIT variants is smaller than that of
 617 Parareal, with the largest speedup of a factor of approximately 1.33. For this non-
 618 linear problem, a slightly larger choice of k than the minimum choice proposed in
 619 [Subsection 3.2](#) gives the best results in terms of runtime. Note that the time for the
 620 setup phase is the same for all variants and is about 2,891 s. Note also that both
 621 algorithms treat the fine level identically, and the improvement comes only from using
 622 local coarse grids instead of one global coarse grid. For comparison, the simulation
 623 time using serial time-stepping on one process is 188,123 s, which is more than two
 624 days. The fastest AT-MGRIT variant needs less than nine hours, which corresponds
 625 to a speedup of a factor of 6.15.

626 **6. Conclusion.** In this paper, we introduce the new AT-MGRIT algorithm, an
 627 iterative parallel-in-time algorithm for solving time-dependent problems. While the
 628 fine level(s) are treated as in the Parareal/MGRIT algorithm, the AT-MGRIT algo-
 629 rithm modifies the coarsest level computations. Instead of considering one global time
 630 grid that covers the entire time interval and is solved sequentially at the coarsest level,
 631 the AT-MGRIT algorithm uses a number of truncated, overlapping local coarse grids,
 632 one for each point on the global coarse grid. Each of these time grids is independent
 633 and covers only a fraction of the global time interval, allowing each problem to be
 634 solved simultaneously and reducing the serial work of the algorithm at the coarsest
 635 level.

636 Theoretical and numerical investigations of the algorithm show that the use of
 637 local coarse grids, which are not all connected to the initial value of the problem, in-
 638 troduces an additional error term compared to classical Parareal/MGRIT, which may
 639 affect the convergence at the beginning of the algorithm. However, the AT-MGRIT
 640 algorithm takes advantage of its iterative nature and eliminates this additional error
 641 term during several iterations, achieving convergence in the same number of iterations

642 as with Parareal/MGRIT while significantly reducing the serial cost on the coarse
 643 level. Simulation of challenging nonlinear problems shows that the MGRIT algorithm
 644 can provide significant speedup compared to Parareal/MGRIT. Future work involves
 645 implementing and studying AT-MGRIT on GPUs and emerging shared-memory com-
 646 puting architectures, where the local and asynchronous aspect of coarse grid solves is
 647 likely to be particularly advantageous.

648 **Appendix A. Error propagation for ideal local coarse problems.** We
 649 consider error-propagation \mathcal{E}_e for one C -point $p = 0, \dots, N_T$ using the ideal local
 650 coarse-grid problem (i.e., exact coarse grid and inverses). The structure of the ma-
 651 trices differs for the first k C -points from all other C -points, since the local coarse
 652 grids corresponding to the first k C -points contain all C -points prior in time. Here,
 653 we want to study the effect of local coarse grids that do not extend back to $t = 0$.
 654 Therefore, we start by considering all local coarse grids $N_T > p \geq k$ and subsequently
 655 discuss the structure for $p < k$. Note that the structure of the matrices of $p = N_T$
 656 is always a submatrix of $N_T > p \geq k$ (see Section 3.1) and therefore is not explicitly
 657 stated. For $N_T > p \geq k$ the matrix $R_I^{(p)} A$ is given by

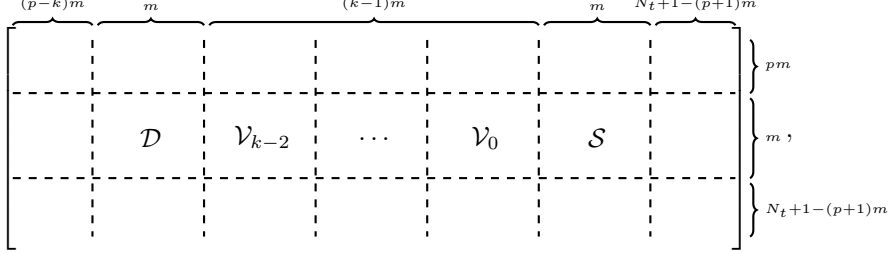
$$658 \quad (A.1) \quad \left[\begin{array}{cccc} \overbrace{\quad}^{(p-k)m} & \overbrace{\quad}^m & \overbrace{\quad}^{km} & \overbrace{\quad}^{N_t+1-(p+1)m} \\ \left[\begin{array}{cccc} \mathbf{0}_{1 \times (m-1)} & -\Phi & I & \mathbf{0}_{1 \times (m-1)} \\ \vdots & \ddots & \ddots & \vdots \\ \mathbf{0}_{1 \times (m-1)} & -\Phi & I & \mathbf{0}_{1 \times (m-1)} \end{array} \right] \end{array} \right]_k,$$

659 which initially contains $(p-k)m + m$ columns corresponding to the omitted points on
 660 the local coarse grid. The following km columns correspond to the C -points present
 661 on the local coarse grid and their corresponding following interval of F -points. Next,
 662 we consider

$$663 \quad P_S^{(p)}(A_c^{(p)})^{-1} = \left[\begin{array}{c} \overbrace{\quad}^k \\ \left[\begin{array}{cccc} \Phi^{(k-1)m} & \dots & \Phi^{2m} & \Phi^m & I \\ \Phi^{(k-1)m+1} & \dots & \Phi^{2m+1} & \Phi^{m+1} & \Phi \\ \vdots & & \vdots & \vdots & \vdots \\ \Phi^{km-1} & \dots & \Phi^{3m-1} & \Phi^{2m-1} & \Phi^{m-1} \end{array} \right] \end{array} \right]_{\begin{array}{c} pm \\ m \\ N_t+1-(p+1)m \end{array}},$$

664 with $A_c^{(p)}$ as in (3.1.1), which defines the effect of selective ideal interpolation multi-
 665 plied by the inverse of the coarse-grid problem. Due to the selective ideal interpolation
 666 operator, exactly m points are considered, namely the C -point to be updated and the
 667 following F -interval consisting of $m - 1$ points. All other points are not changed by
 668 the update of one p and the corresponding rows are therefore zero. As a consequence,
 669 the product $P_S^{(p)}(A_c^{(p)})^{-1}R_I^{(p)}A$ also has only m nonzero rows. Furthermore, we have
 670 exactly $k + 1$ blocks of $m \times m$ matrices which are not equal to zero. The matrix
 671 $P_S^{(p)}(A_c^{(p)})^{-1}R_I^{(p)}A$ in block form is given by

(A.2)

672 

673 with block $m \times m$ inner matrices

674 (A.3)
$$\mathcal{S} = \begin{bmatrix} I & \mathbf{0} & \cdots & \mathbf{0} \\ \Phi & \vdots & & \vdots \\ \vdots & & & \vdots \\ \Phi^{m-1} & \mathbf{0} & \cdots & \mathbf{0} \end{bmatrix}, \quad \mathcal{D} = \begin{bmatrix} \mathbf{0} & \cdots & \mathbf{0} & -\Phi^{(k-1)m+1} \\ \mathbf{0} & \cdots & \mathbf{0} & -\Phi^{(k-1)m+2} \\ \vdots & & \vdots & \vdots \\ \mathbf{0} & \cdots & \mathbf{0} & -\Phi^{km} \end{bmatrix},$$

$$\mathcal{V}_j = \begin{bmatrix} \Phi^{(j+1)m} & \mathbf{0} & \cdots & \mathbf{0} & -\Phi^{jm+1} \\ \Phi^{(j+1)m+1} & \mathbf{0} & \cdots & \mathbf{0} & -\Phi^{jm+2} \\ \vdots & \vdots & & \vdots & \vdots \\ \Phi^{(j+2)m-1} & \mathbf{0} & \cdots & \mathbf{0} & -\Phi^{(j+1)m} \end{bmatrix}.$$

675 Here, \mathcal{D} comes from the truncated coarse-grid points, $\mathcal{V}_{k-2}, \dots, \mathcal{V}_0$ represent the first
 676 $k-1$ local coarse-grid points, and \mathcal{S} corresponds to the last point of the local coarse
 677 grid. Note, the \mathcal{S} -block is the diagonal block of the larger matrix. Now, we consider
 678 the operator PR_I , which is equivalent to an F -relaxation, and globally given by

679
$$PR_I = \begin{bmatrix} \mathcal{S} & & \\ & \ddots & \\ & & \mathcal{S} \end{bmatrix}.$$

680 We can now calculate the error-propagation $(I - \sum_{p=0}^{N_T} P_S^{(p)} (A_c^{(p)})^{-1} R_I^{(p)} A) PR_I$ by ex-
 681 ploring the structure of the matrices $P_S^{(p)} (A_c^{(p)})^{-1} R_I^{(p)} A$ and PR_I . Instead of comput-
 682 ing the complete matrix, we can compute the blocks $-\mathcal{D}\mathcal{S}, -\mathcal{V}_j\mathcal{S}$ for $j = k-2, \dots, 0$,
 683 and $(I - \mathcal{S})\mathcal{S}$. Note that the identity term is added to $-\mathcal{S}$ because \mathcal{S} is the diag-
 684 onal block of $P_S^{(p)} (A_c^{(p)})^{-1} R_I^{(p)} A$. Working through the algebra yields $-\mathcal{V}_j\mathcal{S} = \mathbf{0}$ for
 685 $j = k-2, \dots, 0$, $(I - \mathcal{S})\mathcal{S} = \mathcal{S}^2 - \mathcal{S} = \mathbf{0}$, and the block $m \times m$ matrix

686
$$-\mathcal{D}\mathcal{S} = \begin{bmatrix} \Phi^{km} & \mathbf{0} & \cdots & \mathbf{0} \\ \Phi^{km+1} & \mathbf{0} & \cdots & \mathbf{0} \\ \vdots & \vdots & \vdots & \vdots \\ \Phi^{km+m-1} & \mathbf{0} & \cdots & \mathbf{0} \end{bmatrix},$$

687 which is equivalent to the definition of \mathcal{G} in (3.2). Note that for the case $p < k$ in
 688 matrix (A.2) the operator \mathcal{D} is omitted, since for these C -points all previous C -points
 689 are contained in the local coarse grid.

690 **Appendix B. Error propagation for approximate local coarse problems.**

691 The definition $R_I^{(p)} A$ is the same as in (A.1), but now

$$692 P_S^{(p)} \widetilde{A}_c^{(p)} = \left[\begin{array}{cccc|c} \Phi^0 \Psi^{k-1} & \cdots & \Phi^0 \Psi^2 & \Phi^0 \Psi & \Phi^0 \\ \vdots & & \vdots & \vdots & \vdots \\ \Phi^{m-1} \Psi^{k-1} & \cdots & \Phi^{m-1} \Psi^2 & \Phi^{m-1} \Psi & \Phi^{m-1} \end{array} \right]_{m \times N_t + 1 - (p+1)m}^{k \times pm}.$$

693 As a result, we get a block matrix equivalent to (A.2), but this time with $m \times m$ block
 694 matrices $\widetilde{\mathcal{V}}_j$ and $\widetilde{\mathcal{D}}$ given by

$$695 \widetilde{\mathcal{V}}_j = \begin{bmatrix} \Phi^0 \Psi^{(j+1)} & \mathbf{0} & \cdots & \mathbf{0} & -\Phi^0 \Psi^j \Phi \\ \vdots & \vdots & & \vdots & \vdots \\ \Phi^{m-1} \Psi^{(j+1)} & \mathbf{0} & \cdots & \mathbf{0} & -\Phi^{m-1} \Psi^j \Phi \end{bmatrix} \quad \widetilde{\mathcal{D}} = \begin{bmatrix} \mathbf{0} & \cdots & \mathbf{0} & -\Phi^0 \Psi^{k-1} \Phi \\ \vdots & & \vdots & \vdots \\ \mathbf{0} & \cdots & \mathbf{0} & -\Phi^{m-1} \Psi^{k-1} \Phi \end{bmatrix}$$

696 Note, that \mathcal{S} is the same as given in (A.3). Again, we use the structure of the matrices
 697 and calculate $m \times m$ block submatrices of $P_S^{(p)} (\widetilde{A}_c^{(p)})^{-1} R_I^{(p)} A P R_I$ given by

$$698 -\widetilde{\mathcal{V}}_j \mathcal{S} = \begin{bmatrix} \Phi^0 \Psi^j (\Phi^m - \Psi) & \mathbf{0} & \cdots & \mathbf{0} \\ \vdots & \vdots & \vdots & \vdots \\ \Phi^{m-1} \Psi^j (\Phi^m - \Psi) & \mathbf{0} & \cdots & \mathbf{0} \end{bmatrix} \quad -\widetilde{\mathcal{D}} \mathcal{S} = \begin{bmatrix} \Phi^0 \Psi^{k-1} \Phi^m & \mathbf{0} & \cdots & \mathbf{0} \\ \vdots & \vdots & \vdots & \vdots \\ \Phi^{m-1} \Psi^{k-1} \Phi^m & \mathbf{0} & \cdots & \mathbf{0} \end{bmatrix}$$

699 where $-\widetilde{\mathcal{V}}_j \mathcal{S}$ is equivalent to \mathcal{Z}_j from (3.4) and $-\widetilde{\mathcal{D}} \mathcal{S}$ is equivalent to \mathcal{W} from (3.4).

700 **Appendix C. Discussion spatial parallelism.** Here we demonstrate that the
 701 use of spatial parallelism has comparable effects on sequential time-stepping (before
 702 saturation) as it does on AT-MGRIT. In particular, we emphasize that when spatial
 703 parallelism saturates, the observed near-perfect speedup obtained by spatial parallel-
 704 ism before saturation will extend to AT-MGRIT. Table 5 presents overall runtimes for
 705 using one and four processes in space for time-stepping, Parareal, and two-level AT-
 706 MGRIT, the last two using 64 processes in time (same variants as in Table 1). We see
 707 that for all algorithms we get a speedup of about 3.8 by using four spatial processes
 708 compared to one process. Note that this problem scales well with spatial paralleliza-
 709 tion, and spatial parallelism (as in most cases) should be the first choice. However,
 710 spatial parallelization is exhausted at some point and temporal parallelization can
 711 then provide additional speedups.

712 **Acknowledgments.** We would like to thank Dr. Wayne Mitchell for helpful dis-
 713 cussions that initiated this research. Los Alamos National Laboratory report number
 714 LA-UR-21-26105.

Space processes	Time-stepping one time process	Parareal 64 time processes	Two-level AT-MGRIT 64 time processes
1	347,666 s	91,596 s	79,397 s
4	92,473 s	23,708 s	20,411 s

Table 5: Total runtimes using one and four processes in space for time-stepping, Parareal, and AT-MGRIT with $k = 32$, the latter two using a coarsening factor of 256 and 64 processes in time.

716 [1] S. BALAY, S. ABHYANKAR, M. F. ADAMS, J. BROWN, P. BRUNE, K. BUSCHELMAN, L. DALCIN,
717 A. DENER, V. EIJKHOUT, W. D. GROPP, D. KARPEYEV, D. KAUSHIK, M. G. KNEPLEY,
718 D. A. MAY, L. C. MCINNES, R. T. MILLS, T. MUNSON, K. RUPP, P. SANAN, B. F. SMITH,
719 S. ZAMPINI, H. ZHANG, AND H. ZHANG, *PETSc users manual*, Tech. Report ANL-95/11 -
720 Revision 3.13, Argonne National Laboratory, 2020.

721 [2] R. BANK, R. FALGOUT, T. JONES, T. A. MANTEUFFEL, S. F. MCCORMICK, AND J. W. RUGE,
722 *Algebraic multigrid domain and range decomposition (AMG-DD/AMG-RD)*, SIAM Journal
723 on Scientific Computing, 37 (2015), pp. S113–S136.

724 [3] A. BARTEL, S. BAUMANN, AND S. SCHÖPS, *Structural analysis of electrical circuits including*
725 *magnetoquasistatic devices*, Applied Numerical Mathematics, 61 (2011), pp. 1257–1270.

726 [4] M. BOLTEN, S. FRIEDHOFF, J. HAHNE, AND S. SCHÖPS, *Parallel-in-time simulation of an elec-*
727 *trical machine using MGRIT*, Comput. Vis. Sci., 23 (2020), pp. Paper No. 14, 14.

728 [5] A. BRANDT, *Multi-level adaptive solutions to boundary-value problems*, Mathematics of Com-
729 *putation*, 31 (1977), pp. 333–390.

730 [6] D. CHAZAN AND W. MIRANKER, *Chaotic relaxation*, Linear Algebra and its Applications, 2
731 (1969), pp. 199–222.

732 [7] I. CORTES GARCIA, H. DE GERSEM, AND S. SCHÖPS, *A structural analysis of field/circuit*
733 *coupled problems based on a generalised circuit element*, Numerical Algorithms, (2019),
734 pp. 1–22.

735 [8] F. DANIELI AND S. MACLACHLAN, *Multigrid reduction in time for non-linear hyperbolic equa-*
736 *tions*, 2021, <https://arxiv.org/abs/2104.09404>.

737 [9] V. A. DOBREV, T. KOLEV, N. A. PETERSSON, AND J. B. SCHRODER, *Two-level convergence*
738 *theory for multigrid reduction in time (MGRIT)*, SIAM Journal on Scientific Computing,
739 39 (2017), pp. S501–S527.

740 [10] P. DULAR, C. GEUZAIN, F. HENROTTE, AND W. LEGROS, *A general environment for the*
741 *treatment of discrete problems and its application to the finite element method*, IEEE
742 *Transactions on Magnetics*, 34 (1998), pp. 3395–3398.

743 [11] R. D. FALGOUT, S. FRIEDHOFF, T. KOLEV, S. MACLACHLAN, AND J. B. SCHRODER, *Parallel time*
744 *integration with multigrid*, SIAM Journal on Scientific Computing, 36 (2014), pp. C635–
745 C661.

746 [12] R. D. FALGOUT, M. LECOUVEZ, AND C. S. WOODWARD, *A parallel-in-time algorithm for variable*
747 *step multistep methods*, Journal of Computational Science, 37 (2019), pp. 101029, 12.

748 [13] M. J. GANDER, *50 years of Time Parallel Time Integration*, in *Multiple Shooting and Time*
749 *Domain Decomposition*, Springer, 2015, pp. 69–113.

750 [14] C. GEUZAIN, *GetDP: a general finite-element solver for the de Rham complex*, PAMM, 7
751 (2007), pp. 1010603–1010604.

752 [15] C. GEUZAIN AND J.-F. REMACLE, *Gmsh: A 3-d finite element mesh generator with built-in pre-*
753 *and post-processing facilities*, International Journal for Numerical Methods in Engineering,
754 79 (2009), pp. 1309–1331.

755 [16] C. GEUZAIN AND J.-F. REMACLE, *Gmsh: A three-dimensional finite element mesh genera-*
756 *tor with built-in pre- and post-processing facilities*, 2020. <http://www.gmsh.info>, Online;
757 accessed June 21, 2021.

758 [17] J. GYSELINCK, L. VANDEVELDE, AND J. MELKEBEEK, *Multi-slice FE modeling of electrical*
759 *machines with skewed slots—the skew discretization error*, Magnetics, IEEE Transactions
760 *on*, 37 (2001), pp. 3233 – 3237.

761 [18] J. HAHNE AND S. FRIEDHOFF, *Github repository for PyMGRIT*, 2020. <https://github.com/pymgrit/pymgrit>, Online; accessed June 21, 2021.

762 [19] J. HAHNE, S. FRIEDHOFF, AND M. BOLTEN, *Algorithm 1016: PyMGRIT: A python package for*
763 *the parallel-in-time method mgrid*, ACM Trans. Math. Softw., 47 (2021).

[20] A. HOWSE, H. DE STERCK, R. D. FALGOUT, S. MACLACHLAN, AND J. B. SCHRODER, *Parallel-in-time multigrid with adaptive spatial coarsening for the linear advection and inviscid burgers equations*, SIAM Journal on Scientific Computing, 41 (2019), pp. A538–A565.

[21] J. D. JACKSON, *Classical electrodynamics*, Wiley, New York, NY, 3rd ed., 1998.

[22] L. KRONSJÖ, *A note on the “nested iterations” methods*, Nordisk Tidskr. Informationsbehandling (BIT), 15 (1975), pp. 107–110.

[23] L. KRONSJÖ AND G. DAHLQUIST, *On the design of nested iterations for elliptic difference equations*, Nordisk Tidskr. Informationsbehandling (BIT), 12 (1972), pp. 63–71.

[24] J.-L. LIONS, Y. MADAY, AND G. TURINICI, *Résolution d’EDP par un schéma en temps “pararéel”*, Comptes Rendus de l’Académie des Sciences. Série I. Mathématique, 332 (2001), pp. 661–668.

[25] T. LUNET, J. BODART, S. GRATTON, AND X. VASSEUR, *Time-parallel simulation of the decay of homogeneous turbulence using parareal with spatial coarsening*, Computing and Visualization in Science, 19 (2018), pp. 31–44.

[26] F. MAGOULÈS, G. GBIKPI-BENISSAN, AND Q. ZOU, *Asynchronous iterations of parareal algorithm for option pricing models*, Mathematics, 6 (2018).

[27] W. MITCHELL AND T. MANTEUFFEL, *Advances in implementation, theoretical motivation, and numerical results for the nested iteration with range decomposition algorithm*, Numerical Linear Algebra with Applications, 25 (2018), p. e2149.

[28] W. B. MITCHELL, R. STRZODKA, AND R. D. FALGOUT, *Parallel performance of algebraic multigrid domain decomposition*, Numerical Linear Algebra with Applications, 28 (2021), p. e2342.

[29] A. S. NIELSEN, G. BRUNNER, AND J. S. HESTHAVEN, *Communication-aware adaptive Parareal with application to a nonlinear hyperbolic system of partial differential equations*, Journal of Computational Physics, 371 (2018), pp. 483–505.

[30] J. NIEVERGELT, *Parallel methods for integrating ordinary differential equations*, Comm. ACM, 7 (1964), pp. 731–733.

[31] B. W. ONG AND J. B. SCHRODER, *Applications of time parallelization*, Comput. Vis. Sci., 23 (2020), pp. Paper No. 11, 15.

[32] J. E. PEARSON, *Complex patterns in a simple system*, Science, 261 (1993), pp. 189–192.

[33] M. RIES, U. TROTTERBERG, AND G. WINTER, *A note on MGR methods*, Linear Algebra Appl., 49 (1983), pp. 1–26.

[34] D. RUPRECHT, *Convergence of Parareal with spatial coarsening*, PAMM, 14 (2014), pp. 1031–1034.

[35] S. SCHÖPS, I. NIYONZIMA, AND M. CLEMENS, *Parallel-in-time simulation of eddy current problems using Parareal*, IEEE Transactions on Magnetics, 54 (2018), pp. 1–4.

[36] B. S. SOUTHWORTH, *Necessary conditions and tight two-level convergence bounds for Parareal and Multigrid Reduction in Time*, SIAM Journal on Matrix Analysis and Applications, 40 (2019), pp. 564–608.

[37] B. S. SOUTHWORTH, W. MITCHELL, A. HESSENTHALER, AND F. DANIELI, *Tight two-level convergence of Linear Parareal and MGRIT: Extensions and implications in practice*, arXiv e-prints, (2020). arXiv:2010.11879.

[38] U. TROTTERBERG, C. W. OOSTERLEE, AND A. SCHÜLLER, *Multigrid*, Academic Press, London, 2001.

[39] Q. ZOU, G. GBIKPI-BENISSAN, AND F. MAGOULÈS, *Asynchronous parareal algorithm applied to european option pricing*, in 2017 16th International Symposium on Distributed Computing and Applications to Business, Engineering and Science (DCABES), 2017, pp. 37–40.